

Steady-State Rate-Optimal Power Adaptation in Energy Harvesting Opportunistic Cognitive Radios with Spectrum Sensing and Channel Estimation Errors

Hassan Yazdani, Azadeh Vosoughi, *Senior Member, IEEE*

Abstract—We consider an uplink cognitive radio (CR) network that can access a wideband spectrum licensed to a primary network, which is divided into non-overlapping narrowband channels. The secondary users (SUs) are equipped with rechargeable battery of finite capacity that solely powered by energy harvesting from the ambient environment. The SUs which are aware of the available energy in their batteries, sense the activity of the primary transmitter. If the result of spectrum sensing is idle, SUs send pilot symbols to the secondary access point (AP) and AP estimates the secondary channel power. Then, AP feeds back the channel gain to SUs. Knowing the battery state and the feedback information, SUs optimally adapt their transmit power to AP such that the steady-state sum rate of SU-AP link is maximized, subject to average interference constraint (AIC) imposed on the primary receiver and the causality constraint of the batteries. We illustrate the effect of the AIC, energy arrival rate and battery capacity on the steady state distribution of battery, CR network rate, battery energy outage probability and transmission outage probability via simulation.

Index Terms—opportunistic cognitive radio, energy harvesting, imperfect spectrum sensing, imperfect channel estimation, constrained sum rate maximization, average interference power constraint, finite-size battery, steady-state battery operation, adaptive transmission power.

I. INTRODUCTION

A. Literature Review

The explosive rise in demand for high data rate wireless applications has turned the spectrum into a scarce resource. Cognitive radio (CR) technology is a promising solution which alleviates spectrum scarcity problem by allowing an unlicensed (secondary) user to access licensed frequency bands in a such way that its imposed interference on the primary users (PUs) is limited [1], [2]. Therefore, CR systems can increase spectrum efficiency significantly. CR systems are mainly classified as underlay CR and opportunistic CR systems. In underlay CR systems, SUs use a licensed frequency band simultaneously with PUs, conditioned that the interference power imposed on PUs (caused by SUs) remains below a pre-determined level. In opportunistic CR systems, SUs use a licensed frequency band as long as the frequency band is not used by PUs. While opportunistic CR systems do not require coordination between PUs and SUs to acquire channel state information (CSI) corresponding to SU-PU link, they necessitate spectrum

sensing to monitor and detect PUs' activities and protect PUs against harmful interference caused by SUs [3]–[5].

In these systems, the status of PUs' activities (being busy or idle) and the duration of spectrum sensing affect the system performance [4]–[8]. Spectrum sensing is prone to errors characterized in terms of mis-detection and false alarm probabilities which need to be considered in the CR system design. Another important factor that impacts the performance of CR systems is the level of assumption made regarding the availability of CSI. In opportunistic CR systems, although CSI corresponding to SU-PU link is not required (which is a major advantage), still CSI corresponding to SU_{tx} - SU_{rx} is needed for properly adapting the data transmission.

In addition to spectral efficiency, energy efficiency is another important metric to consider when designing communication systems [9]–[15]. Energy harvesting (EH) has been recognized as an effective approach for improving the energy efficiency. EH-powered devices can operate without the need for external power cables or periodic battery replacements [16], [17]. EH-enabled CR systems have received substantial attention as a promising solution for increasing both energy efficiency and spectral efficiency [18]–[20]. EH-enabled communication systems can harvest energy from ambient energy sources (e.g., solar, wind, thermal, vibration) or radio frequency (RF) signals. For instance, in an ambient RF EH-enabled system, the energy of emitted RF signals from TV/radio broadcast towers, cellular base stations, and Wi-Fi points is captured by SU transmitter (SU_{tx}) antenna and stored in its battery [21]–[25]. A dedicated RF signal source can be utilized for energy harvesting and enabling and simultaneous wireless information and power transfer (SWIPT) systems [26], [27].

The body of research on EH-enabled communication systems can be grouped into two main categories depending on the adopted energy arrival model [9], [28]: in the first model, the energy arrival is deterministic and the transmitter has a causal or non-causal knowledge of the energy arrival at the beginning of transmission [29]. In the second model, the energy arrival is stochastic. In practice, the energy arrival of ambient energy sources, including ambient RF signal sources, is intrinsically time-variant and often sporadic. This natural factor degrades the performance of the battery-free EH-enabled communication systems in which a “harvest-then-transmit” strategy is adopted, i.e., users can only transmit when the energy harvested in one time slot is sufficient for

data transmission [30]. To flatten the randomness effect of the energy arrival, the harvested energy can be stored in a battery, to balance the energy arrival and the energy consumption. In practice, the capacity of the energy storage devices is limited, and this can result in an energy overflow.

Power/energy management in EH-enabled communication systems with battery is necessary in order to adapt the rate of energy consumption with the rate of energy harvesting. If the energy management policy is overly aggressive, such that the rate of energy consumption is greater than the rate of energy harvesting, the transmitter may stop functioning, due to energy outage. On the other hand, if the energy management policy is overly conservative, the transmitter may fail to utilize the excess energy, due to energy overflow, and the data transmission would become limited in each energy allocation interval.

Focusing on opportunistic EH-enabled CR systems, we realize that power control strategies, aiming at optimizing the performance of SUs, should be designed such that spectrum sensing (and its errors) as well as spectrum sensing-data transmission tradeoffs are incorporated in the design process. Furthermore, these power control strategies should depend on the level of assumption regarding CSI of SU_{tx} - SU_{rx} and whether the adapted transmit power levels are continuous or discrete values. For instance, the authors in [21] considered a system model, where depending on the results of spectrum sensing, SU_{tx} harvests energy (when the spectrum is sensed busy) or SU_{tx} transmits data (when the spectrum is sensed idle), and aimed at maximizing the SU channel capacity, via optimizing the threshold of the energy detector (employed for spectrum sensing). Aiming at a similar goal (i.e., maximizing the SU's channel capacity), the authors in [25] investigated an optimal mode selection policy (whether to access the spectrum or to harvest energy) for CR sensor networks. In addition to the transmit power, the energy allocation for sensing is considered in an energy harvesting sensor node with a finite data buffer in [15] and [6]. The authors in [7] formulated the problem differently, as they separated energy harvesting phase and spectrum sensing phase. Targeting to maximize the SU's throughput, via optimizing spectrum sensing duration and the threshold of the energy detector, the authors in [7] investigated the energy harvesting-spectrum sensing-data transmission tradeoffs.

The authors in [31] aimed at maximizing the SU's bit rate, via adapting data transmit power and modulation order, according to CSI of SU_{tx} - SU_{rx} link and the SU_{tx} battery state. In [31] the authors assumed CSI is perfectly known at both SU_{tx} and SU_{rx} and the optimized power levels at SU_{tx} are discrete (based on quantized CSI). In practice, only partial CSI can be available due to several factors (e.g., channel estimation error, mobility of receiver, and limitation of feedback channel from receiver to SU_{tx}). Partial (imperfect) CSI has deteriorating effects on the CR system performance and should not be overlooked. For instance, the authors in [28], [32] analyzed maximizing the average throughput of SU, in two asymptotic regimes (where the rate of energy harvesting is very small and very large), via optimizing the transmit power. In [28], [32] the authors assumed partial CSI

at SU_{tx} (due to channel estimation error), whereas perfect CSI is available at SU_{rx} . In [29], the authors targeted maximizing the SU's throughput, via optimizing the channel threshold and transmission power. In [29] the authors assumed partial 1-bit CSI at SU_{tx} (due to the limitation of feedback channel), whereas perfect CSI is available at SU_{rx} .

B. Knowledge Gap and Our Contributions

To the best of our knowledge, our work is the first to consider the combined effects of spectrum sensing error and imperfect CSI of SUs-AP links on the achievable sum rate of an opportunistic EH-enabled CR network with a stochastic energy harvesting model and battery with finite capacity. Integrating the energy harvesting devices at CR systems with imperfect spectrum sensing and imperfect CSI presents new challenges. Hence, one needs to study the combined impacts of all of these factors on the system performance.

We consider an opportunistic CR network consisting of N_u SUs and an access point (AP), where each SU is equipped with a rechargeable battery of finite capacity. The SUs are solely powered by energy harvesting and the batteries are replenished by a stochastic energy harvesting process. We concentrate on the design of energy scheduling policies using natural ambient energy sources and we assume SUs can harvest energy and send data at the same time and there is no battery leakage. In our system, SU_n first senses the spectrum for a duration of τ_s seconds. If the spectrum is sensed idle, SU_n sends pilot symbols to the AP and AP estimates the SU_n -AP channel gain. Then, AP feeds back the channel, over an error-free feedback link to SU_n . Note that imperfect CSI of SU_n -AP link due to channel estimation error (even under perfect spectrum sensing) has negative influence on the link rate. Imperfect spectrum sensing exacerbates the negative effect of imperfect CSI on the link rate. Since the (imperfect) channel gain between SU_n and AP is available at SU_n , SU_n can adapt its data transmit power according to the available energy in its battery as well as the channel gain.

Our main contributions follow:

- 1) The dynamic behaviors of the SUs' battery is modeled as a finite state Markov chain. The effect of PU activity, battery capacity, spectrum sensing error, channel estimation error as well as the stochastic distribution of harvested energy is considered in the model and its steady state distribution is attained.
- 2) Given this system model, we establish a lower bound on the achievable sum rate of SUs-AP links, in the presence of both spectrum sensing error and channel estimation error. We formulate a novel constrained optimization problem, aiming at maximizing the derived lower bound, subject to AIC imposed on PU and the causality constraint of the battery.
- 3) We propose a power adaptation strategy for SU_n that mimics the behavior of the rate-optimal power adaptation scheme with respect to the channel power gain \hat{g}_n , i.e., when the \hat{g}_n is smaller than a cut-off threshold θ_n , the transmit energy is zero, and when the \hat{g}_n exceeds θ_n , the transmit (which is proportional to a parameter Ω_n) energy increases monotonically as \hat{g}_n increases.

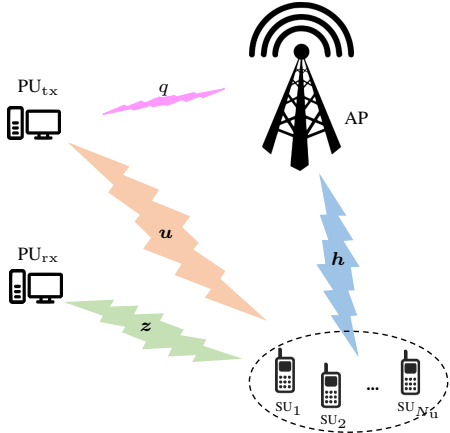


Fig. 1: Schematics of the uplink CR network.

- 4) We find the optimal values of the parameters Ω_n and θ_n such that the steady-state sum rate of the CR network is maximized.
- 5) We derive closed form expressions for the battery outage probability and transmission outage probability and show the behavior of them with respect to simulation parameters.

C. Paper Organization

The remainder of the paper is organized as follows. Section II explains our system model. In Section III we describe our binary energy-based detector for detecting PU activity and in Section IV describes the channel probing phase. In Section V we explain the data transmission phase and obtain the rate of our network. Section VI presents our simulation results and Section VII concludes the paper.

II. SYSTEM MODEL

We consider an uplink CR network that can access a wideband spectrum licensed to a primary network, which is divided into M non-overlapping narrowband spectrum bands. The primary network consists of a primary transmitter (PU_{tx}) and a primary receiver (PU_{rx}). The secondary network consists of an access point (AP) and N_u secondary users (see Fig. 1). The AP can serve up to M SUs simultaneously and we assume that $N_u \leq M$. We also assume that narrowband spectrum bands are pre-assigned to SUs and thus each SU knows which band to sense and transmit data over. The SUs are equipped with identical energy harvesting circuits to harvest energy from the ambient environment and identical finite size batteries for energy storage (see Fig. 2). We consider block fading channel model and suppose flat fading coefficients from PU_{tx} to SU_n, PU_{tx} to AP, SU_n to PU_{rx}, and, SU_n to AP are four independent zero-mean complex Gaussian random variables, which we denote by u_n , q , z_n and h_n with variances δ_{u_n} , δ_q , δ_{z_n} and γ_n , respectively.

A. Battery and Energy Harvesting Models

We assume that SUs operate under a time-slotted scheme, with slot duration of T_f seconds, and they always have data

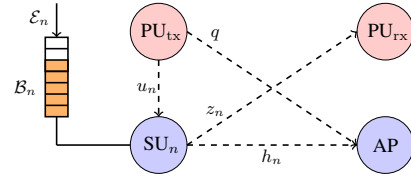


Fig. 2: Our CR system model corresponding to SU_n for $n = 1, \dots, N_u$.

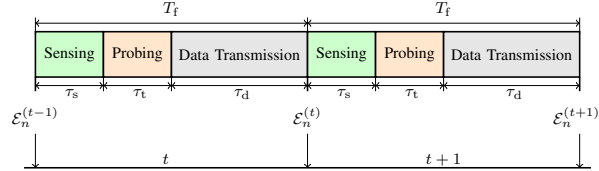


Fig. 3: Slot structure of SUs.

to transmit. Each time slot is indexed by an integer t for $t = 1, 2, \dots$. The energy harvester at each SU stores randomly arrived energy in a finite size battery and consumes the stored energy for spectrum sensing, channel probing, and data transmission. Each battery consists of K cells (units) and the amount of energy stored in each unit is equal to e_u Joules. Thus, the battery can store up to Ke_u Joules of energy.

When k cells of the battery is charged (the amount of stored energy in the battery is ke_u Joules) we say that the battery is at state k . Let $\mathcal{B}_n^{(t)} \in \{0, 1, \dots, K\}$ denote the discrete random process indicating the battery state of SU_n at the beginning of time slot t . We define the probability mass function (pmf) of the discrete random variable $\mathcal{B}_n^{(t)}$ as $\zeta_{k,n}^{(t)} = \Pr(\mathcal{B}_n^{(t)} = k)$, where $\sum_{k=0}^K \zeta_{k,n}^{(t)} = 1$. Note that $\mathcal{B}_n^{(t)} = 0$ and $\mathcal{B}_n^{(t)} = K$ represent the empty battery and full battery levels, respectively.

Let $\mathcal{E}_n^{(t)}$ denote the randomly arriving energy packets during time slot t of SU_n, where the energy packet measured in Jules is e_u Jules. The discrete random process $\mathcal{E}_n^{(t)}$ is typically modeled as a sequence of independent and identically distributed (i.i.d.) random variables [15], regardless of the spectrum occupancy state of PU_{tx}. We assume that the discrete random variables $\mathcal{E}_n^{(t)}$'s are i.i.d. over time and independent across sensors. We model $\mathcal{E}_n^{(t)}$ as a Poisson random variable with the pmf $f_{\mathcal{E}_n}(r) = \Pr(\mathcal{E}_n = r) = e^{-\rho_n} \rho_n^r / r!$ for $r = 0, 1, \dots, \infty$, where ρ_n denotes the average arriving energy. Let $\alpha_{h_n}^{(t)}$ be the number of stored (harvested) energy units in the battery at SU_n during time slot t . This harvested energy cannot be used during time slot t . Since the battery has a finite capacity of K cells, $\alpha_{h_n}^{(t)} \in \{0, 1, \dots, K\}$. Also, $\alpha_{h_n}^{(t)}$ are i.i.d. over time slots and independent across sensors. Let $f_{\alpha_{h_n}}(r) = \Pr(\alpha_{h_n} = r)$ denote the pmf of $\alpha_{h_n}^{(t)}$. We can find the pmf of $\alpha_{h_n}^{(t)}$ in terms of the pmf of $\mathcal{E}_n^{(t)}$ as the following

$$f_{\alpha_{h_n}}(r) = \begin{cases} f_{\mathcal{E}_n}(r), & \text{if } 0 \leq r \leq K-1 \\ \sum_{m=K}^{\infty} f_{\mathcal{E}_n}(m), & \text{if } r = K. \end{cases} \quad (1)$$

B. Slot Structure of SUs

Each time slot consists of three sub-slots (see Fig. 3), corresponding to spectrum sensing phase, channel probing

phase, and data transmission phase, with fixed durations of $\tau_s = N_s/f_s$, $\tau_t = N_t/f_s$, $\tau_d = N_d/f_s$, respectively. Note that f_s is the sampling frequency, N_s is the number of collected samples during spectrum sensing phase, N_t is the number of training symbols sent during channel probing phase, and N_d is the number of data symbols sent during data transmission phase. Also, we have $T_f = \tau_s + \tau_t + \tau_d$.

During *spectrum sensing phase*, SU_n senses its pre-assigned single spectrum band to detect PU_{tx} 's activity. We model the PU_{tx} 's activity in each spectrum band as a Bernoulli random variable and we assume the statistics of PU_{tx} are i.i.d. across M spectrum bands and over time slots. Therefore, we can frame the spectrum sensing problem at SU_n as a binary hypothesis testing problem. Suppose $\mathcal{H}_1^{(t)}$ and $\mathcal{H}_0^{(t)}$ represent the binary hypotheses of PU_{tx} being active and inactive in time slot t , respectively, with prior probabilities $\Pr\{\mathcal{H}_1^{(t)}\} = \pi_1$ and $\Pr\{\mathcal{H}_0^{(t)}\} = \pi_0$. SU_n applies a binary detection rule to decide whether or not PU_{tx} is active in its pre-assigned band. Let $\widehat{\mathcal{H}}_{0,n}$ and $\widehat{\mathcal{H}}_{1,n}$, with probabilities $\widehat{\pi}_{0,n} = \Pr\{\widehat{\mathcal{H}}_{0,n}\}$ and $\widehat{\pi}_{1,n} = \Pr\{\widehat{\mathcal{H}}_{1,n}\}$ denote the SU_n detector outcome, i.e., the detector finds PU_{tx} active and inactive (the result of spectrum sensing is busy or idle), respectively. The accuracy of this binary detector is characterized by its false alarm and detection probabilities. The details of the binary detector are presented in Section III.

Depending on the outcome of spectrum sensing, SU_n stays in spectrum sensing phase or enters *channel probing phase*. In this phase, SU_n sends N_t training symbols with fixed symbol power $P_t = \alpha_t e_u / \tau_t$, to enable channel estimation at the AP, where α_t is the number of consumed cells of energy for channel probing¹. We assume that the battery always has α_t units of stored energy for channel probing. Let $h_n^{(t)}$ denote the SU_n -AP fading coefficient in time slot t and $g_n^{(t)} = |h_n^{(t)}|^2$ be the corresponding channel power gain. Using the received signals corresponding to the training symbols, the AP estimates $\widehat{h}_n^{(t)}$ and lets $\widehat{g}_n^{(t)} = |\widehat{h}_n^{(t)}|^2$ and shares this value with SU_n via a feedback channel. Next, SU_n enters *data transmission phase*. During this phase, SU_n sends N_d Gaussian data symbols with adaptive symbol power according to its battery state and the received information via the feedback channel about SU_n -AP link. If the battery is at state k , then SU_n allocates $\alpha_{k,n}$ cells of stored energy for each data symbol transmission, implying that the adaptive symbol power is $P_{k,n}^{(t)} = \alpha_{k,n}^{(t)} p_u$, where $p_u = e_u / \tau_d$. Note that since $\alpha_{k,n}^{(t)}$ is discrete, $P_{k,n}^{(t)}$ is discrete. The details of the choice of $\alpha_{k,n}^{(t)}$ according to the battery state k and the feedback information \widehat{g}_n are given in Section II-C and the details of channel estimation are explained in Section IV.

C. Transmission Model and Battery Dynamics

As we said, we assume that SU_n adapts its transmit energy per data symbol (power) according to its battery state k and

¹For ease of presentation, we assume that circuit power (energy) consumption is negligible in comparison to the consumed energy for channel probing and data transmission. Otherwise, it can easily be incorporated into the system model.

the received information via the feedback channel about its channel power gain \widehat{g}_n . In particular, we choose a power adaptation strategy that mimics the behavior of the rate-optimal power adaptation scheme with respect to the channel power gain [5], i.e., when \widehat{g}_n is smaller than a cut-off threshold θ_n (to be optimized), the transmit energy is zero, and when \widehat{g}_n exceeds θ_n , the transmit energy increases monotonically as \widehat{g}_n increases until it reaches its maximum value of $\lfloor k\Omega_n \rfloor - \alpha_t$, where $\Omega_n \in [0, 1]$ (to be optimized), and $\lfloor \cdot \rfloor$ denotes the floor function. Mathematically, we express $\alpha_{k,n}^{(t)}$ for SU_n as the following

$$\alpha_{k,n}^{(t)} = \max \{ \overline{\alpha}_{k,n}^{(t)}, 0 \}, \quad \text{for } k = 0, 1, \dots, K, \quad (2a)$$

$$\overline{\alpha}_{k,n}^{(t)} = \left\lfloor \Omega_n k \left(1 - \frac{\theta_n}{\widehat{g}_n^{(t)}} \right)^+ \right\rfloor - \alpha_t, \quad (2b)$$

where $(x)^+ = \max\{x, 0\}$. The parameter Ω_n in (2) adapts the energy consumption with the energy harvesting rate. If we increase Ω_n , such that the rate of energy consumption is greater than the rate of energy harvesting, the transmitter may stop functioning, due to the energy outage. On the other hand, if Ω_n is too small, the transmitter may fail to utilize the excess energy, due to energy overflow, and the data transmission would become limited in each energy allocation interval. Note that $\overline{\alpha}_{k,n}^{(t)}$ in (2) ensures that the battery always has α_t units of stored energy for channel probing. Furthermore, the transmission policy in (2) satisfies the causality constraint of the battery. The causality constraint restrains the energy corresponding to symbol transmit power to be less than the available stored energy in the battery, i.e., $\alpha_{k,n} \leq k - \alpha_t$. Note that $\alpha_{k,n}$ is discrete random variable and $\alpha_{k,n} \in \{0, 1, \dots, K\}$. Let $\psi_{i,k,n}^\varepsilon = \Pr(\alpha_{k,n} = i | \mathcal{H}_\varepsilon)$ denote the pmf of $\alpha_{k,n}$ given \mathcal{H}_ε , $\varepsilon = 0, 1$. We have

$$\psi_{i,k,n}^\varepsilon = \begin{cases} 1, & \text{if } 0 \leq k \leq \alpha_t, i = 0 \\ 0, & \text{if } 0 \leq k \leq \alpha_t, i \neq 0 \\ Y_{k,n}, & \text{if } k \geq \alpha_t + 1, i = 0 \\ Q_{i,k,n}, & \text{if } k \geq \alpha_t + 1, 1 \leq i \leq \lfloor k\Omega_n \rfloor - \alpha_t \\ 0, & \text{if } k \geq \alpha_t + 1, i \geq \lfloor k\Omega_n \rfloor - \alpha_t + 1 \end{cases} \quad (3)$$

in which

$$Q_{i,k,n} = F_{\widehat{g}_n}^\varepsilon(c_{i,k,n}) - F_{\widehat{g}_n}^\varepsilon(a_{i,k,n}) \quad (4a)$$

$$Y_{k,n} = F_{\widehat{g}_n}^\varepsilon(\theta_n) + \sum_{m=1}^{\min(\lfloor k\Omega_n \rfloor, \alpha_t)} Q_{m-\alpha_t, k, n} \quad (4b)$$

$$a_{i,k,n} = \frac{\theta_n k \Omega_n}{k \Omega_n - \alpha_t - i}, \quad c_{i,k,n} = \frac{\theta_n k \Omega_n}{k \Omega_n - \alpha_t - i - 1}, \quad (4c)$$

where $F_{\widehat{g}_n}^\varepsilon(x) = F_{\widehat{g}_n}(x | \mathcal{H}_\varepsilon)$ is the cumulative distribution function (CDF) of \widehat{g}_n given \mathcal{H}_ε . Note that if $c_{i,k,n} < 0$, we set $c_{i,k,n} = +\infty$.

The battery state at the beginning of time slot $t+1$ depends on the battery state at the beginning of time slot t , the harvested energy during time slot t , the transmission symbol, as well as α_t . In particular, if at time slot t , SU_n senses its spectrum band to be idle, the state of its battery at the

$$\phi_{0,j}^n = \sum_{l=0}^K \left[\psi_{l,j,n}^0 \widehat{\pi}_{0,n} F_{\alpha_{h_n}}(\alpha_t + l - j) \right] + \widehat{\pi}_{1,n} F_{\alpha_{h_n}}(-j) \quad (7a)$$

$$\phi_{K,j}^n = \sum_{l=0}^K \left[\psi_{l,j,n}^0 \widehat{\pi}_{0,n} \left(1 - F_{\alpha_{h_n}}(\alpha_t + l + K - j) \right) \right] + \widehat{\pi}_{1,n} \left(1 - F_{\alpha_{h_n}}(K - j) \right) \quad (7b)$$

$$\phi_{i,j}^n = \sum_{l=0}^K \left[\psi_{l,j,n}^0 \widehat{\pi}_{0,n} f_{\alpha_{h_n}}(\alpha_t + l + i - j) \right] + \widehat{\pi}_{1,n} f_{\alpha_{h_n}}(i - j), \quad \text{for } i = 1, \dots, K - 1 \quad (7c)$$

beginning of slot $t + 1$ is

$$\mathcal{B}_n^{(t+1)} = \min \left\{ \left(\mathcal{B}_n^{(t)} - \alpha_t - \alpha_{k,n}^{(t)} + \alpha_{h_n}^{(t)} \right)^+, K \right\}, \quad (5)$$

On the other hand if at time slot t , SU _{n} senses its spectrum band to be busy, the state of its battery at the beginning of slot $t + 1$ is

$$\mathcal{B}_n^{(t+1)} = \min \left\{ \left(\mathcal{B}_n^{(t)} + \alpha_{h_n}^{(t)} \right)^+, K \right\}, \quad (6)$$

since $\alpha_{k,n}^{(t)} = 0$. Considering the dynamic battery state model in (5) and (6) we note that, conditioned on $\alpha_{h_n}^{(t)}$ and $\alpha_{k,n}^{(t)}$ the value of $\mathcal{B}_n^{(t+1)}$ only depends on the value of $\mathcal{B}_n^{(t)}$ (and not the battery states of time slots before t). Hence, the battery state random process $\mathcal{B}_n^{(t)}$ can be modeled as a Markov chain. Let the probability vector of battery state in time slot t be $\zeta_n^{(t)} = [\zeta_{1,n}^{(t)}, \dots, \zeta_{K,n}^{(t)}]^T$. Note that the probability $\zeta_{k,n}^{(t)}$ depends on the battery state at slot $t - 1$, the number of battery units filled by the harvested energy during slot $t - 1$, the probability of spectrum band sensed idle, and, the number of energy units allocated for data transmission at slot $t - 1$ when the spectrum band is sensed idle, i.e., $\zeta_{k,n}^{(t)}$ depends on $\mathcal{B}_n^{(t-1)}, \alpha_{h_n}^{(t-1)}, \widehat{\pi}_{0,n}, \alpha_{k,n}^{(t-1)}$, respectively. Assuming the Markov chain is time-homogeneous, we let Φ_n denote the $(K + 1) \times (K + 1)$ transition probability matrix of this chain with its (i, j) -th entry $\phi_{i,j}^n = \Pr(\mathcal{B}_n^{(t)} = i | \mathcal{B}_n^{(t-1)} = j)$ given in (7) where $F_{\alpha_{h_n}}(\cdot)$ is the commutative distribution function (CDF) of α_{h_n} . We have

$$\zeta_n^{(t+1)} = \Phi_n \zeta_n^{(t)} \quad (8)$$

Since the Markov chain characterized by the transition probability matrix Φ_n is irreducible and aperiodic, there exists a unique steady state distribution, regardless of the initial state [33]. Let $\zeta_n = \lim_{t \rightarrow \infty} \zeta_n^{(t)}$ be the unique steady state probability vector. This vector satisfies the following equations

$$\zeta_n = \Phi_n \zeta_n, \quad (9a)$$

$$\zeta_n^T \mathbf{1} = \sum_{k=1}^K \zeta_{k,n} = 1, \quad (9b)$$

where $\mathbf{1}$ is an all-ones vector, i.e., ζ_n is the normalized eigenvector corresponding to the unit eigenvalue of Φ_n , such that the entries of ζ_n sums up to one. The closed-form

expression for ζ_n is [34]

$$\zeta_n = (\Phi_n - \mathbf{I} + \mathbf{B})^{-1} \mathbf{1}, \quad (10)$$

where \mathbf{B} is an all-ones matrix and \mathbf{I} is the identity matrix. From this point forward, we assume that the battery is at its steady state and we drop the superscript t .

To illustrate our transmission model in (2) we consider the following simple numerical example. Assuming that the battery has $K = 7$ cells, Fig. 4 shows an example of $\alpha_{k,n}$ for our CR system for two sets of $\{\Omega_n, \theta_n\}$ given as $\Omega_n^{(a)} = 0.75, \theta_n^{(a)} = 0.02$ and $\Omega_n^{(b)} = 0.95, \theta_n^{(b)} = 0.05$. The corresponding transition probability matrices are given in the following

$$\Phi_n^{(a)} = \begin{pmatrix} 0.42 & 0.29 & 0.17 & 0.08 & 0.02 & 0 & 0 & 0 \\ 0.12 & 0.13 & 0.12 & 0.09 & 0.05 & 0.02 & 0 & 0 \\ 0.19 & 0.12 & 0.13 & 0.12 & 0.09 & 0.05 & 0.02 & 0 \\ 0.07 & 0.19 & 0.12 & 0.13 & 0.12 & 0.09 & 0.05 & 0.02 \\ 0.05 & 0.07 & 0.19 & 0.12 & 0.13 & 0.12 & 0.09 & 0.05 \\ 0.05 & 0.05 & 0.07 & 0.19 & 0.12 & 0.13 & 0.12 & 0.09 \\ 0.04 & 0.05 & 0.05 & 0.07 & 0.19 & 0.12 & 0.13 & 0.12 \\ 0.06 & 0.1 & 0.15 & 0.2 & 0.27 & 0.46 & 0.58 & 0.71 \end{pmatrix}$$

$$\Phi_n^{(b)} = \begin{pmatrix} 0.51 & 0.4 & 0.28 & 0.16 & 0.08 & 0.02 & 0 & 0 \\ 0.17 & 0.11 & 0.12 & 0.12 & 0.09 & 0.05 & 0.02 & 0 \\ 0.06 & 0.17 & 0.11 & 0.12 & 0.12 & 0.09 & 0.05 & 0.02 \\ 0.05 & 0.06 & 0.17 & 0.11 & 0.12 & 0.12 & 0.09 & 0.05 \\ 0.05 & 0.05 & 0.06 & 0.17 & 0.11 & 0.12 & 0.12 & 0.09 \\ 0.05 & 0.05 & 0.05 & 0.06 & 0.17 & 0.11 & 0.12 & 0.12 \\ 0.04 & 0.05 & 0.05 & 0.05 & 0.06 & 0.17 & 0.11 & 0.12 \\ 0.06 & 0.11 & 0.16 & 0.21 & 0.26 & 0.32 & 0.49 & 0.6 \end{pmatrix}$$

Our goal is to find the transmission parameters $\{\Omega_n, \theta_n\}$ in (2b) for all SUs such that the sum rate of our CR network is maximized, subject to a constraint on the average interference power that collective SUs can impose on PU_{rx}. We assume that this optimization problem is solved offline at AP, given the statistical information of fading channels, the number of samples collected during spectrum sensing phase N_s , the number of training symbols sent during channel probing phase N_t , and power of training symbols P_t . The solutions to this optimization problem, i.e., the optimal set $\{\Omega_n, \theta_n\}_{n=1}^{N_u}$ is available a priori at the AP and SUs, to be utilized for adapting symbol power during data transmission phase. The idea of offline power allocation optimization with a limited feedback channel has been used before for distributed detection systems

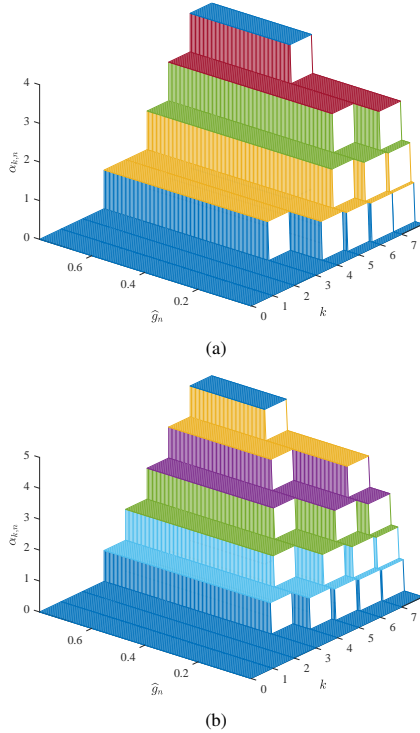


Fig. 4: This example shows how many energy units ($\alpha_{k,n}$) SU_n spends for data transmission, given its battery state and the received information about its channel gain via feedback link. (a) $\Omega_n^{(a)} = 0.75$, $\theta_n^{(a)} = 0.02$, (b) $\Omega_n^{(b)} = 0.95$, $\theta_n^{(b)} = 0.05$.

in wireless sensor networks [35]. In the following sections, we describe how SUs operate during spectrum sensing phase, channel probing phase, and data transmission phase. For the readers' convenience, we have collected the most commonly used symbols in Table I.

TABLE I: Most commonly used symbols.

Symbol	Description
N_s	Number of collected samples during <i>spectrum sensing phase</i>
N_t	Number of training symbols during <i>channel probing phase</i>
N_d	Number of data symbols during <i>data transmission phase</i>
P_t	Power of training symbols
$h_n, \hat{h}_n, \tilde{h}_n$	Fading coefficient of SU_n -AP link, LMMSE channel estimate, and its corresponding estimation error
$\gamma_n, \hat{\gamma}_n, \tilde{\gamma}_n$	Variances of $h_n, \hat{h}_n, \tilde{h}_n$
π_0, π_1	Prior probabilities of \mathcal{H}_0 and \mathcal{H}_1
$\hat{\pi}_{0,n}, \hat{\pi}_{1,n}$	Probabilities of spectrum bands being sensed idle or busy
$\zeta_{k,n}$	Probability of SU_n battery being at state k
u_n	Fading coefficient of PU _{tx} - SU_n link with variance δ_{u_n}
q	Fading coefficient of PU _{tx} -AP link with variance δ_q
z_n	Fading coefficient of SU_n -PU _{rx} link with variance δ_{z_n}

III. SPECTRUM SENSING PHASE

In order to access its spectrum band, SU_n first needs to sense its band during spectrum sensing phase, to determine whether it is busy or idle (see Fig. 3). We formulate the spectrum sensing at SU_n as a binary hypothesis testing problem, where the received signal at SU_n can be written as:

$$\begin{aligned} \mathcal{H}_0 &: y_n[m] = w_n[m], \\ \mathcal{H}_1 &: y_n[m] = u_n[m] p[m] + w_n[m], \end{aligned} \quad (12)$$

for $m = 1, \dots, N_s$, where $p[m]$ is the transmit signal of PU_{tx}, $w_n[m] \sim \mathcal{CN}(0, \sigma_{w_n}^2)$ is the additive white Gaussian

noise (AWGN) at SU_n and $u_n[m]$ is the fading coefficient corresponding to PU_{tx}- SU_n channel. The two hypotheses \mathcal{H}_0 and \mathcal{H}_1 with probabilities π_0 and $\pi_1 = 1 - \pi_0$ denote the spectrum is truly idle and truly busy, respectively. We assume that π_0 and π_1 are known to SUs based on long-term spectrum measurements. For spectrum sensing we consider energy detector, where the decision statistics at SU_n is $Z_n = \frac{1}{N_s} \sum_{m=1}^{N_s} |y_n[m]|^2$. The accuracy of this detector is characterized by its false alarm probability $P_{fa_n} = \Pr(\hat{\mathcal{H}}_{1,n} | \mathcal{H}_0) = \Pr(Z_n > \xi_n | \mathcal{H}_0)$ and detection probability $P_{d_n} = \Pr(\hat{\mathcal{H}}_{1,n} | \mathcal{H}_1) = \Pr(Z_n > \xi_n | \mathcal{H}_1)$, where ξ_n is the local decision threshold. For large N_s , we can invoke central limit theorem and approximate the cumulative distribution function (CDF) of Z_n as Gaussian. Hence, P_{fa_n} and P_{d_n} can be expressed in terms of Q function as below [36]

$$P_{fa_n} = Q\left(\left(\frac{\xi_n}{\sigma_{w_n}^2} - 1\right)\sqrt{N_s}\right), \quad P_{d_n} = Q\left(\left(\frac{\xi_n}{\sigma_{w_n}^2} - \nu_n - 1\right)\sqrt{\frac{N_s}{2\nu_n + 1}}\right),$$

where $\nu_n = P_p \delta_{u_n} / \sigma_{w_n}^2$ and P_p is the average transmit power of PU_{tx}. For a given value of $P_{d_n} = \bar{P}_d$, the false alarm probability can be written as

$$P_{fa_n} = Q\left(\sqrt{2\nu_n + 1} Q^{-1}(\bar{P}_d) + \nu_n \sqrt{\tau_s f_s}\right). \quad (13)$$

The probabilities $\hat{\pi}_{0,n}$ and $\hat{\pi}_{1,n}$, are related to P_{d_n} and P_{fa_n} . In particular, we have $\hat{\pi}_{0,n} = \beta_{0,n} + \beta_{1,n}$ and $\hat{\pi}_{1,n} = 1 - \hat{\pi}_{0,n}$, where

$$\beta_{0,n} = \Pr\{\mathcal{H}_0, \hat{\mathcal{H}}_{0,n}\} = \pi_0(1 - P_{fa_n}), \quad (14a)$$

$$\beta_{1,n} = \Pr\{\mathcal{H}_1, \hat{\mathcal{H}}_{0,n}\} = \pi_1(1 - P_{d_n}). \quad (14b)$$

IV. CHANNEL PROBING PHASE

Depending on the outcome of its spectrum sensing, SU_n either stays in spectrum sensing phase (i.e., remains silent in the remaining of time slot) if its band is sensed busy (the detector outcome is $\hat{\mathcal{H}}_{1,n}$), or it enters channel probing phase if its band is sensed idle (the detector outcome is $\hat{\mathcal{H}}_{0,n}$). During channel probing phase, we assume SU_n sends training vector $\mathbf{x}_t = \sqrt{P_t} \mathbf{1}$, where $\mathbf{1}$ is an $N_t \times 1$ all-ones vector to enable channel estimation at the AP. Let vector $\mathbf{s}_n = [s_n(1), \dots, s_n(N_t)]^T$ denote the discrete-time representation of received training symbols at the AP from SU_n . Assuming the fading coefficient h_n corresponding to SU_n -AP channel is unchanged during the entire time slot, we have

$$\begin{aligned} \mathcal{H}_0, \hat{\mathcal{H}}_{0,n} &: s_n[m] = h_n \sqrt{P_t} + v_n[m], \\ \mathcal{H}_1, \hat{\mathcal{H}}_{0,n} &: s_n[m] = h_n \sqrt{P_t} + q[m] p[m] + v_n[m], \end{aligned} \quad (15)$$

for $m = 1, \dots, N_t$, $v_n[m] \sim \mathcal{CN}(0, \sigma_{v_n}^2)$ is the AWGN at the AP, and $q[m]$ is the fading coefficient corresponding to PU_{tx}-AP channel. The linear minimum mean square error (LMMSE) estimate of h_n given $\hat{\mathcal{H}}_{0,n}$ is [5], [37]

$$\hat{h}_n = C_{h_n \mathbf{s}_n} C_{\mathbf{s}_n}^{-1} \mathbf{s}_n, \quad (16a)$$

$$C_{h_n \mathbf{s}_n} = \mathbb{E}\{h_n \mathbf{s}_n^H | \hat{\mathcal{H}}_{0,n}\} = \gamma_n \sqrt{P_t} \mathbf{1}, \quad (16b)$$

$$\begin{aligned} C_{\mathbf{s}_n} &= \mathbb{E}\{\mathbf{s}_n \mathbf{s}_n^H | \hat{\mathcal{H}}_{0,n}\} = \omega_{0,n} \mathbb{E}\{\mathbf{s}_n \mathbf{s}_n^H | \mathcal{H}_0, \hat{\mathcal{H}}_{0,n}\} \\ &\quad + \omega_{1,n} \mathbb{E}\{\mathbf{s}_n \mathbf{s}_n^H | \mathcal{H}_1, \hat{\mathcal{H}}_{0,n}\}, \end{aligned} \quad (16c)$$

where

$$\omega_{0,n} = \Pr\{\mathcal{H}_0|\widehat{\mathcal{H}}_{0,n}\} = \frac{\pi_0(1-P_{\text{fa}_n})}{\widehat{\pi}_{0,n}} = \frac{\beta_{0,n}}{\widehat{\pi}_{0,n}}, \quad (17a)$$

$$\omega_{1,n} = \Pr\{\mathcal{H}_1|\widehat{\mathcal{H}}_{0,n}\} = \frac{\pi_1(1-P_{\text{d}_n})}{\widehat{\pi}_{0,n}} = \frac{\beta_{1,n}}{\widehat{\pi}_{0,n}}, \quad (17b)$$

and

$$\mathbb{E}\{\mathbf{s}_n \mathbf{s}_n^H | \mathcal{H}_0, \widehat{\mathcal{H}}_{0,n}\} = (\widehat{\gamma}_n^0 P_{\text{t}} + \sigma_{v_n}^2) \mathbf{I}, \quad (18a)$$

$$\mathbb{E}\{\mathbf{s}_n \mathbf{s}_n^H | \mathcal{H}_1, \widehat{\mathcal{H}}_{0,n}\} = (\widehat{\gamma}_n^1 P_{\text{t}} + \sigma_{v_n}^2 + \sigma_p^2) \mathbf{I}. \quad (18b)$$

After substituting (17) into (16), \widehat{h}_n reduces to

$$\widehat{h}_n = \frac{\gamma_n \sqrt{P_{\text{t}}}}{\gamma_n P_{\text{t}} N_{\text{t}} + \sigma_{v_n}^2 + \omega_{1,n} \sigma_p^2} \sum_{m=1}^{N_{\text{t}}} s_n[m], \quad (19)$$

where $\sigma_{\mathcal{E}}^2 = P_{\text{p}} \delta_q$. The estimation error is $\tilde{h}_n = h_n - \widehat{h}_n$, where \widehat{h}_n and h_n are orthogonal random variables [37], and \widehat{h}_n and \tilde{h}_n are zero mean. Approximating $q[m]p[m]$ as a zero-mean Gaussian random variable with variance σ_p^2 , we find that the estimate \widehat{h}_n given $\widehat{\mathcal{H}}_{0,n}$ is distributed as a Gaussian mixture random variable [5]. Let $\widehat{\gamma}_n$ and $\tilde{\gamma}_n$ represent the variances of \widehat{h}_n and \tilde{h}_n , respectively. Also, Let $\widehat{\gamma}_n^0$ and $\widehat{\gamma}_n^1$ represent the variances of \widehat{h}_n under $\{\mathcal{H}_0, \widehat{\mathcal{H}}_{0,n}\}$ and $\{\mathcal{H}_1, \widehat{\mathcal{H}}_{0,n}\}$, respectively. We have

$$\begin{aligned} \widehat{\gamma}_n^0 &= \text{VAR}\{\widehat{h}_n | \mathcal{H}_0, \widehat{\mathcal{H}}_{0,n}\} = \frac{\gamma_n^2 P_{\text{t}} N_{\text{t}} (\gamma_n P_{\text{t}} N_{\text{t}} + \sigma_{v_n}^2)}{(\gamma_n P_{\text{t}} N_{\text{t}} + \sigma_{v_n}^2 + \omega_{1,n} \sigma_p^2)^2}, \\ \widehat{\gamma}_n^1 &= \text{VAR}\{\widehat{h}_n | \mathcal{H}_1, \widehat{\mathcal{H}}_{0,n}\} = \frac{\gamma_n^2 P_{\text{t}} N_{\text{t}} (\gamma_n P_{\text{t}} N_{\text{t}} + \sigma_{v_n}^2 + \sigma_p^2)}{(\gamma_n P_{\text{t}} N_{\text{t}} + \sigma_{v_n}^2 + \omega_{1,n} \sigma_p^2)^2}. \end{aligned}$$

Therefore, $\widehat{\gamma}_n = \omega_{0,n} \widehat{\gamma}_n^0 + \omega_{1,n} \widehat{\gamma}_n^1$. Also, let $\tilde{\gamma}_n^0$ and $\tilde{\gamma}_n^1$ indicate the variances of \tilde{h}_n under $\{\mathcal{H}_0, \widehat{\mathcal{H}}_{0,n}\}$ and $\{\mathcal{H}_1, \widehat{\mathcal{H}}_{0,n}\}$, respectively. We have

$$\tilde{\gamma}_n^0 = \text{VAR}\{\tilde{h}_n | \mathcal{H}_0, \widehat{\mathcal{H}}_{0,n}\} = \gamma_n - \widehat{\gamma}_n^0, \quad (21a)$$

$$\tilde{\gamma}_n^1 = \text{VAR}\{\tilde{h}_n | \mathcal{H}_1, \widehat{\mathcal{H}}_{0,n}\} = \gamma_n - \widehat{\gamma}_n^1. \quad (21b)$$

Hence, $\tilde{\gamma}_n = \omega_{0,n} \tilde{\gamma}_n^0 + \omega_{1,n} \tilde{\gamma}_n^1$. For ideal spectrum sensing, we get $\omega_{0,n} = 1$ and $\omega_{1,n} = 0$ and \widehat{h}_n becomes Gaussian. Let $F_{\widehat{g}_n}^{\varepsilon}(x)$ denote the CDF of \widehat{g}_n under $\{\mathcal{H}_{\varepsilon}, \widehat{\mathcal{H}}_{0,n}\}$ for $\varepsilon = 0, 1$. Note that under $\{\mathcal{H}_{\varepsilon}, \widehat{\mathcal{H}}_{0,n}\}$ for $\varepsilon = 0, 1$, \widehat{h}_n is zero mean complex Gaussian. Hence, under $\{\mathcal{H}_{\varepsilon}, \widehat{\mathcal{H}}_{0,n}\}$ for $\varepsilon = 0, 1$, \widehat{g}_n is an exponential random variable with mean $\widehat{\gamma}_n^{\varepsilon}$ and CDF

$$F_{\widehat{g}_n}^{\varepsilon}(x) = 1 - e^{-\frac{x}{\widehat{\gamma}_n^{\varepsilon}}}. \quad (22)$$

The CDF of \widehat{g}_n , denoted as $F_{\widehat{g}_n}^{\varepsilon}(x)$, can be expressed in terms of $F_{\widehat{g}_n}^0(x)$ and $F_{\widehat{g}_n}^1(x)$ as the following:

$$F_{\widehat{g}_n}(x) = \omega_{0,n} F_{\widehat{g}_n}^0(x) + \omega_{1,n} F_{\widehat{g}_n}^1(x). \quad (23)$$

After channel estimation, the AP feeds back the channel gains $\widehat{g}_n = |\widehat{h}_n|^2$ over a feedback link to SU_n .

V. DATA TRANSMISSION PHASE

After channel probing phase, SU_n enters this phase. We note that entering this phase is only possible, if in spectrum sensing phase the outcome of the binary detector is $\widehat{\mathcal{H}}_{0,n}$. During

this phase, SU_n sends Gaussian data symbols to the AP, while it adapts its transmission power according to information provided by the AP through the feedback channel about SU_n -AP link as well as its battery state. In particular, SU_n transmits N_{d} zero-mean i.i.d. complex Gaussian symbols $x_n[m]$ for $m = 1, \dots, N_{\text{d}}$ with power $P_{k,n} = \alpha_{k,n} p_{\text{u}}$, when the battery is at state k and $\alpha_{k,n}$ is given in (2). Let $s_n[m]$ denote the discrete-time representation of received signal at the AP from SU_n . Due to error in spectrum sensing, we need to distinguish the signal model for $s_n[m]$ under \mathcal{H}_0 and \mathcal{H}_1 . We have

$$\mathcal{H}_0, \widehat{\mathcal{H}}_{0,n}: s_n[m] = h_n x_n[m] + v_n[m], \quad (24)$$

$$\mathcal{H}_1, \widehat{\mathcal{H}}_{0,n}: s_n[m] = h_n x_n[m] + q[m] p[m] + v_n[m],$$

Substituting $h_n = \widehat{h}_n + \tilde{h}_n$ in (24), we reach at

$$\begin{aligned} \mathcal{H}_0, \widehat{\mathcal{H}}_{0,n}: s_n[m] &= \widehat{h}_n x_n[m] + \tilde{h}_n x_n[m] + v_n[m], \\ \mathcal{H}_1, \widehat{\mathcal{H}}_{0,n}: s_n[m] &= \widehat{h}_n x_n[m] + \tilde{h}_n x_n[m] + \underbrace{q[m] p[m] + v_n[m]}_{\text{new noise } \eta_{n,1}[m]}. \end{aligned} \quad (25)$$

where the new noise terms depend on \tilde{h}_n . Given \widehat{g}_n at the AP, we obtain an achievable rate expression for a time slot by considering symbol-wise mutual information between channel input and output over the duration of N_{d} data symbols as follows

$$\begin{aligned} R_n &= \frac{D_{\text{d}}}{N_{\text{d}}} \sum_{m=1}^{N_{\text{d}}} \left[\beta_{0,n} \mathbb{E} \left\{ I(x_n[m]; s_n[m] | \widehat{g}_n, \mathcal{H}_0, \widehat{\mathcal{H}}_{0,n}) \right\} \right. \\ &\quad \left. + \beta_{1,n} \mathbb{E} \left\{ I(x_n[m]; s_n[m] | \widehat{g}_n, \mathcal{H}_1, \widehat{\mathcal{H}}_{0,n}) \right\} \right], \end{aligned} \quad (26)$$

where $D_{\text{d}} = \tau_{\text{d}}/T_{\text{f}}$ is the fraction of the time slot used for data transmission and the expectations in (26) are taken over the conditional probability density functions (pdfs) of \widehat{g}_n given $\{\mathcal{H}_{\varepsilon}, \widehat{\mathcal{H}}_{0,n}\}$ for $\varepsilon = 0, 1$. To characterize R_n in (26) we need to find $\mathbb{E}\{I(x_n[m]; s_n[m] | \widehat{g}_n, \mathcal{H}_{\varepsilon}, \widehat{\mathcal{H}}_{0,n})\}$. Exploiting the chain rule we can rewrite this expectation as follows

$$\begin{aligned} &\mathbb{E} \left\{ I(x_n[m]; s_n[m] | \widehat{g}_n, \mathcal{H}_{\varepsilon}, \widehat{\mathcal{H}}_{0,n}) \right\} \\ &= \sum_{k=0}^K \zeta_{k,n} I(x_n[m]; s_n[m] | \widehat{g}_n, k, \mathcal{H}_{\varepsilon}, \widehat{\mathcal{H}}_{0,n}) \end{aligned} \quad (27)$$

Note that $I(x_n[m]; s_n[m] | \widehat{g}_n, \mathcal{H}_{\varepsilon}, \widehat{\mathcal{H}}_{0,n})$ in (27) is the mutual information between $x_n[m]$ and $s_n[m]$ when the battery state is k , given \widehat{g}_n and $\{\mathcal{H}_{\varepsilon}, \widehat{\mathcal{H}}_{0,n}\}$. From now on, we drop the variable m in $x_n[m]$ and $s_n[m]$ for brevity of the presentation. Focusing on $I(x_n; s_n | \widehat{g}_n, \mathcal{H}_{\varepsilon}, \widehat{\mathcal{H}}_{0,n})$, we have

$$\begin{aligned} I(x_n; s_n | \widehat{g}_n, k, \mathcal{H}_{\varepsilon}, \widehat{\mathcal{H}}_{0,n}) &= h(x_n | \widehat{g}_n, k, \widehat{\mathcal{H}}_{0,n}, \mathcal{H}_{\varepsilon}) \\ &\quad - h(x_n | s_n, \widehat{g}_n, k, \widehat{\mathcal{H}}_{0,n}, \mathcal{H}_{\varepsilon}), \end{aligned} \quad (28)$$

where $h(\cdot)$ is the differential entropy. Consider the first term in (28). Since $x_n \sim \mathcal{CN}(0, P_{k,n})$ we have $h(x_n | \widehat{g}_n, k, \widehat{\mathcal{H}}_{0,n}, \mathcal{H}_{\varepsilon}) = \log_2(\pi e P_{k,n})$. Consider the second term in (28). Due to channel estimation error, the new noises

$\eta_{n,\varepsilon}$'s in (25) are non-Gaussian and this term does not have a closed form expression. Hence, similar to [38]–[40] we employ bounding techniques to find an upper bound on this term. This term is upper bounded by the entropy of a Gaussian random variable with the variance $\Theta_M^{n,\varepsilon}$

$$\Theta_M^{n,\varepsilon} = \mathbb{E} \left\{ |x_n - \mathbb{E}\{x_n | \hat{g}_n, k, \hat{\mathcal{H}}_{0,n}, \mathcal{H}_\varepsilon\}|^2 \right\}, \quad (29)$$

where the expectations are taken over the conditional pdf of x_n given $s_n, \hat{g}_n, k, \hat{\mathcal{H}}_{0,n}, \mathcal{H}_\varepsilon$. In fact, $\Theta_M^{i,\varepsilon}$ is the mean square error (MSE) of the MMSE estimate of x_n given $s_n, \hat{g}_n, k, \hat{\mathcal{H}}_{0,n}, \mathcal{H}_\varepsilon$. Using minimum variance property of MMSE estimator, we have $\Theta_M^{n,\varepsilon} \leq \Theta_L^{n,\varepsilon}$, where $\Theta_L^{n,\varepsilon}$ is the MSE of the LMMSE estimate of x_n given $s_n, \hat{g}_n, k, \hat{\mathcal{H}}_{0,n}, \mathcal{H}_\varepsilon$. Combining all, we find $h(x_n | s_n, \hat{g}_n, k, \hat{\mathcal{H}}_{0,n}, \mathcal{H}_\varepsilon) \leq \log_2(\pi e \Theta_L^{n,\varepsilon})$ and $I(x_n; s_n | \hat{g}_n, k, \hat{\mathcal{H}}_{0,n}, \mathcal{H}_\varepsilon) \geq \log_2(P_{k,n} / \Theta_L^{n,\varepsilon})$ where

$$\Theta_L^{n,\varepsilon} = \frac{P_{k,n} \sigma_{\eta_{n,\varepsilon}}^2}{\sigma_{\eta_{n,\varepsilon}}^2 + \hat{g}_n P_{k,n}}, \quad (30)$$

$$\sigma_{\eta_{n,\varepsilon}}^2 = \tilde{\gamma}_n^{\varepsilon} P_{k,n} + \sigma_{v_n}^2 + \varepsilon \sigma_p^2. \quad (31)$$

At the end, we obtain the lower bounds as follow

$$I(x_n; s_n | \hat{g}_n, k, \hat{\mathcal{H}}_{0,n}, \mathcal{H}_0) \geq \log_2(1 + \hat{g}_n b_{k,n}^0), \quad (32a)$$

$$I(x_n; s_n | \hat{g}_n, k, \hat{\mathcal{H}}_{0,n}, \mathcal{H}_1) \geq \log_2(1 + \hat{g}_n b_{k,n}^1). \quad (32b)$$

where

$$b_{k,n}^0 = \frac{P_{k,n}}{(\tilde{\gamma}_n^0 P_{k,n} + \sigma_{v_n}^2)}, \quad b_{k,n}^1 = \frac{P_{k,n}}{(\tilde{\gamma}_n^1 P_{k,n} + \sigma_{v_n}^2 + \sigma_p^2)}. \quad (33)$$

Substituting equations (27) and (32) in (26) and noting that the symbol-wise mutual information between channel input and output for N_d data symbols are equal we reach at

$$\begin{aligned} R_n \geq R_{n,\text{LB}} &= D_d \beta_{0,n} \sum_{k=0}^K \zeta_{k,n} \mathbb{E} \left\{ \log_2(1 + \hat{g}_n b_{k,n}^0) | \mathcal{H}_0 \right\} \\ &+ D_d \beta_{1,n} \sum_{k=0}^K \zeta_{k,n} \mathbb{E} \left\{ \log_2(1 + \hat{g}_n b_{k,n}^1) | \mathcal{H}_1 \right\}, \end{aligned} \quad (34)$$

Next, we compute the conditional expectations in (34), in which we take average over \hat{g}_n , given \mathcal{H}_ε . Using (3) and (4c) we have

$$\begin{aligned} &\mathbb{E} \left\{ \log_2(1 + \hat{g}_n b_{k,n}^{\varepsilon}) | \mathcal{H}_\varepsilon \right\} \\ &= \sum_{i=1}^{\lfloor k \Omega_n \rfloor - \alpha_t} \int_{a_{i,k,n}}^{c_{i,k,n}} \log_2(1 + S_{i,n}^{\varepsilon} x) f_{\hat{g}_n}(x) dx \\ &= \sum_{i=1}^{\lfloor k \Omega_n \rfloor - \alpha_t} V_k(S_{i,n}^{\varepsilon}, \tilde{\gamma}_n^{\varepsilon}) \end{aligned} \quad (35a)$$

in which

$$S_{i,n}^0 = \frac{i p_u}{(\tilde{\gamma}_n^0 i p_u + \sigma_{v_n}^2)}, \quad S_{i,n}^1 = \frac{i p_u}{(\tilde{\gamma}_n^1 i p_u + \sigma_{v_n}^2 + \sigma_p^2)}, \quad (35b)$$

$$V_k(S_{i,n}, \tilde{\gamma}_n) = M(c_{i,k,n}, S_{i,n}, \tilde{\gamma}_n) - M(a_{i,k,n}, S_{i,n}, \tilde{\gamma}_n), \quad (35c)$$

and

$$\begin{aligned} M(x, S, w) &= \int \log_2(1 + Sx) \frac{e^{-\frac{x}{w}}}{w} dx \\ &= \frac{e^{\frac{1}{Sw}}}{\ln(2)} \text{Ei}\left(\frac{-x}{w} - \frac{1}{Sw}\right) - e^{\frac{-x}{w}} \log_2(1 + Sx). \end{aligned} \quad (36)$$

Also, $c_{i,k,n}$ and $a_{i,k,n}$ are given in (4c). Substituting (35a) in (34) we reach to

$$\begin{aligned} R_{n,\text{LB}} &= D_d \beta_{0,n} \sum_{k=\alpha_t+1}^K \sum_{i=1}^{\lfloor k \Omega_n \rfloor - \alpha_t} \zeta_{k,n} V_k(S_{i,n}^0, \tilde{\gamma}_n^0) \\ &+ D_d \beta_{1,n} \sum_{k=\alpha_t+1}^K \sum_{i=1}^{\lfloor k \Omega_n \rfloor - \alpha_t} \zeta_{k,n} V_k(S_{i,n}^1, \tilde{\gamma}_n^1) \end{aligned} \quad (37)$$

We note that the lower bounds in (32) are achieved when the new noises $\eta_{n,0}, \eta_{n,1}$ in (25) are regarded as worst-case Gaussian noise and hence the MMSE and LMMSE of x_n given $s_n, \hat{g}_n, k, \hat{\mathcal{H}}_{0,n}, \mathcal{H}_\varepsilon$ coincide. Given the rate lower bound $R_{n,\text{LB}}$ for SU_n, the sum rate lower bound for all SU_n's is

$$R_{\text{LB}} = \sum_{n=1}^{N_u} R_{n,\text{LB}}. \quad (38)$$

So far, we have established a sum rate lower bound on the achievable sum rate. Next, we characterize the average inference constraint (AIC). Suppose \bar{I}_{av} is the maximum allowed average interference power, i.e., the average interference power that collective SUs impose on PU_{rx} cannot exceed \bar{I}_{av} . To satisfy AIC, we have

$$\sum_{n=1}^{N_u} \beta_{1,n} \mathbb{E}\{z_n\} \left[D_d \mathbb{E}\{P_n(\hat{g}_n)\} + D_t P_t \right] \leq \bar{I}_{\text{av}}. \quad (39)$$

where $D_t = \tau_t / T_f$ and the expectation is over the conditional pdfs of \hat{g}_n under $\{\mathcal{H}_1, \hat{\mathcal{H}}_{0,n}\}$. The first term in (39) is the average interference power imposed on PU_{rx} when SUs transmit data symbols, and the second term is the average interference imposed on PU_{rx} when SUs send training symbols for channel estimation at the AP. Using (3) we compute the term with expectation inside (39) as follows

$$\begin{aligned} \mathbb{E}\{P_n(\hat{g}_n)\} &= \sum_{k=0}^K \zeta_{k,n} \sum_{i=0}^K \Pr(\alpha_{k,n} = i | \mathcal{H}_1) i p_u \\ &= \sum_{k=\alpha_t+1}^K \zeta_{k,n} \sum_{i=1}^{\lfloor k \Omega_n \rfloor - \alpha_t} \psi_{i,k,n}^1 i p_u \end{aligned} \quad (40)$$

Substituting (40) into (39), we can rewrite the AIC in (39) as

$$\sum_{n=1}^{N_u} \beta_{1,n} \delta_{z_n} \left[\sum_{k=\alpha_t+1}^K \zeta_{k,n} \sum_{i=1}^{\lfloor k \Omega_n \rfloor - \alpha_t} \psi_{i,k,n}^1 i p_u + D_t P_t \right] \leq \bar{I}_{\text{av}}. \quad (41)$$

For ideal spectrum sensing we get $\beta_{1,n} = 0$ in (14), implying that data transmission from SUs to the AP does not cause interference on PU_{rx} and the left-hand side of (41) becomes zero, i.e., the AIC is always satisfied.

Next, we examine how spectrum sensing error and channel estimation error affect R_{LB} and AIC expressions. First, spec-

TABLE II: Simulation Parameters

Parameter	Value	Parameter	Value
P_p	1 watts	$\sigma_{v_n}^2$	1
π_0	0.7	$\sigma_{w_n}^2$	1
τ_t	0.1 ms	α_t	1
τ_s	1 ms	\bar{P}_d	0.85
T_f	10 ms	f_s	20 KHz
e_u	0.01	δ_q	1

trum sensing error affects AIC via $\beta_{1,n}$, and R_{LB} via $\beta_{0,n}$ and $\beta_{1,n}$. Recall $\beta_{0,n}, \beta_{1,n}$ depend on $\pi_0, P_{f_{a,n}}, P_{d_n}$ (see (14)). Second, channel estimation error affects AIC via $D_t, \psi_{i,k,n}^1$, and R_{LB} via $\tilde{\gamma}_n^\varepsilon$.

Having the mathematical expressions for R_{LB} and AIC, our goal is to optimize the set of transmission parameters $\{\Omega_n, \theta_n\}$ for all SUs such that R_{LB} is maximized, subject to the AIC. To inspect the underlying trade-offs between decreasing the average interference power imposed by SU_n 's on PU_{rx} and increasing the sum rate lower bound R_{LB} , we note that increasing data symbol transmission power $P_{k,n}$ increases R_{LB} . However, it increases the average interference power. Aiming to strike a balance between increasing R_{LB} and decreasing the imposed average interference power, we seek the optimal $\{\Omega_n, \theta_n\}_{n=1}^{N_u}$ such that R_{LB} in (34) is maximized, subject to AIC given in (41). In other words, we are interested in solving the following constrained optimization problem

$$\begin{aligned} & \underset{\{\Omega_n, \theta_n\}_{n=1}^{N_u}}{\text{Maximize}} \quad R_{LB} \\ & \text{s.t.: } \Omega_n \in [0, 1], \\ & \theta_n \geq 0, \\ & \text{AIC in (41) is satisfied.} \end{aligned} \quad (42)$$

We note that solving (42) requires an $2N_u$ -dimensional search over the search space $[0, 1]^{N_u} \times [0, \infty]^{N_u}$.

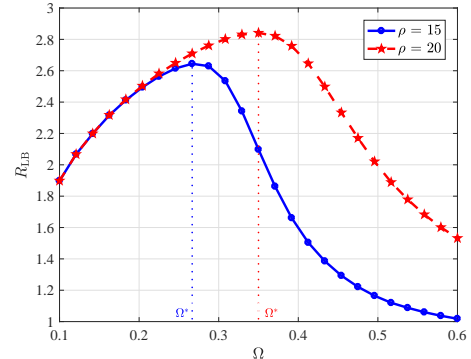
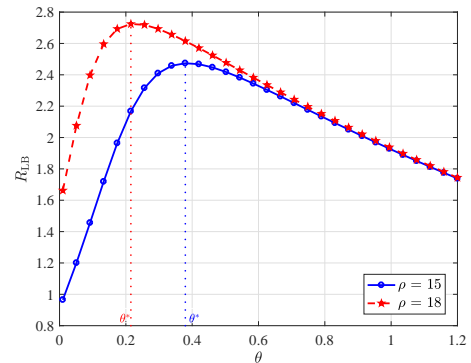
VI. SIMULATION RESULTS

We corroborate our analysis on constrained maximization of achievable sum rate lower bound with Matlab simulations. Our simulation parameters are given in Table II.

• **Effect of Ω, θ :** First, we assume there is a single SU and we illustrate how $\zeta_{k,n}$, R_{LB} in (38), and $P_{b_n}^{Out}$ defined below depend on the optimization variables Ω_n and θ_n . We define the battery outage probability $P_{b_n}^{Out}$ as the steady state probability of battery being equal or lower than α_t . When a battery is at outage, it cannot yield energy for data transmission. We have

$$P_{b_n}^{Out} = \Pr(b_n \leq \alpha_t) = \sum_{k=0}^{\alpha_t} \zeta_{k,n} \quad (43)$$

For $N_u = 1$, we let $\gamma = 2, \delta_u = 1, \delta_z = 1$. Fig. 5 illustrates the effect of Ω on the rate R_{LB} for two values of ρ . As we observe, R_{LB} is not a convex nor a concave function of Ω . For small Ω , as Ω increases (until Ω^*), R_{LB} increases because the harvested energy can recharge the battery and yields more power for transmission. However, when Ω goes further than Ω^* , the stored energy (or equivalently the harvested energy) cannot support the transmission and R_{LB} decreases. Moreover,

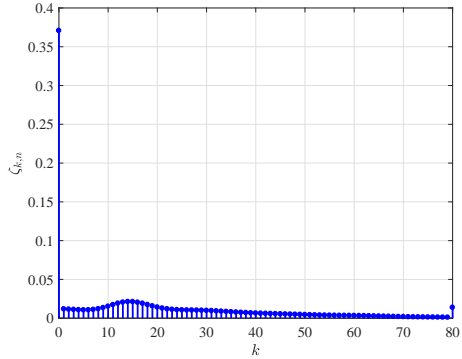
Fig. 5: R_{LB} versus Ω for $K = 80, \theta = 0.2$.Fig. 6: R_{LB} versus θ for $K = 80, \Omega = 0.35$.

when the energy harvesting rate ρ increases, a higher rate can be achieved. The behavior of R_{LB} versus the cut-off threshold θ is shown in Fig. 6 for two values of ρ . We observe that, like Ω , there is a an optimal value of θ which yields the maximum R_{LB} . As we observe, R_{LB} is not a convex nor a concave function of θ .

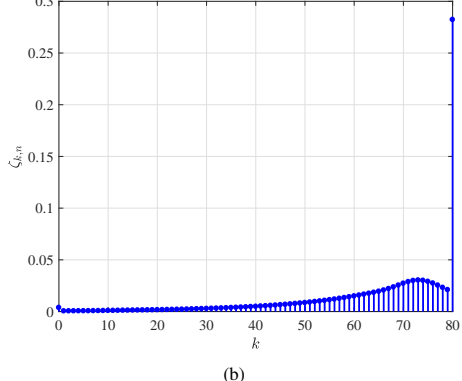
For comparison, the steady state battery probability (Pmf of battery) for two values of Ω is shown in Fig. 7. We define the available average battery energy for SU_n as

$$\bar{b}_n = \mathbb{E}\{b_n\} = \sum_{k=0}^K k \zeta_{k,n} \quad (44)$$

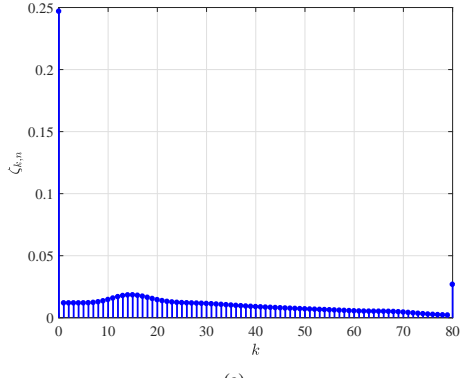
We observe that for high Ω (Fig. 7a), the battery almost get discharged and we have $\bar{b}^{(a)} = 16.97$. On the other hand, for small Ω (Fig. 7b), $\bar{b}^{(b)} = 66.30$, we do not utilize the excessive energy in the battery and as a result, the data rate is limited. Hence, we need to find the best value for Ω to impose a balance between the available energy and data rate so that we can achieve the highest data rate. The steady state battery probability for two values of θ are shown in Figs. 8a and 8b with $\bar{b}^{(a)} = 24.08, \bar{b}^{(b)} = 71.55$. For a fixed Ω , as the cut-off threshold θ increases, SU_{tx} transmits a lower power to PU_{rx} . Hence, for small θ (less than θ^*), the transmit power is high and the battery cannot yield enough energy for transmission. As a result, at the steady state, the battery discharges. On the other hand, for high θ , SU_{tx} transmits a lower power and do not utilizes the excessive energy in the battery. As a result the data rate is limited and we need to find the best value for θ to impose a balance between the available energy and data rate.



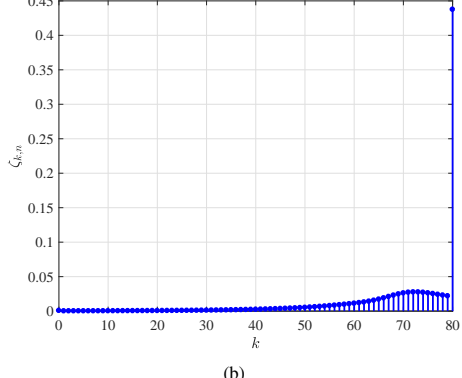
(a)



(b)

Fig. 7: $\zeta_{k,n}$ versus k for $K = 80$, $\rho = 15$, $\theta = 0.2$, (a) $\Omega = 0.45$, (b) $\Omega = 0.30$.

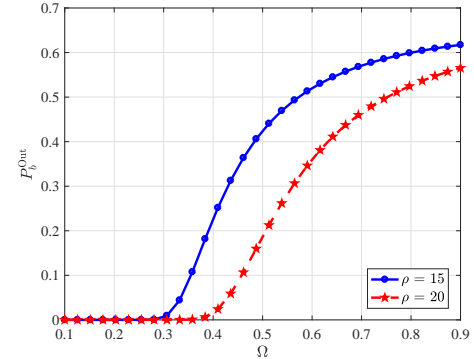
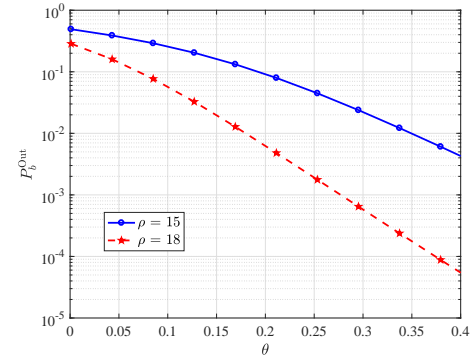
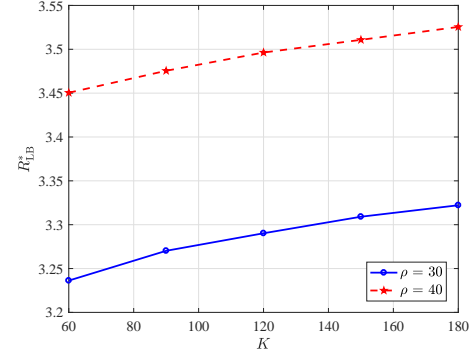
(a)



(b)

Fig. 8: $\zeta_{k,n}$ versus k for $K = 80$, $\rho = 15$, $\Omega = 0.35$, (a) $\theta = 0.1$, (b) $\theta = 0.5$.

Fig. 9 illustrates the behavior of P_b^{Out} versus Ω for a fixed θ . It can be seen that as Ω increases, the battery cannot support the required power for data transmission and the steady state

Fig. 9: P_b^{Out} versus Ω for $K = 80$, $\theta = 0.05$.Fig. 10: P_b^{Out} versus θ for $K = 80$, $\Omega = 0.35$.Fig. 11: R_{LB}^* versus K for $\bar{T}_{\text{av}} = \infty$.

outage probability of battery increases. The behavior of P_b^{Out} versus θ is illustrated in Fig. 10 for a fixed Ω . As θ , the transmit power decreases and the probability of battery being in outage decreases as well.

• **Optimized R_{LB}^* :** Next, we consider solving the constrained optimization problem in (42) and plot the maximized R_{LB} , denoted as R_{LB}^* (R_{LB}^* is R_{LB} evaluated at the solutions obtained from solving (42)). Fig. 11 depicts R_{LB}^* versus the battery capacity K for $N_u = 3$, the fading parameters $\gamma = [2, 2.2, 2.1]$, $\delta_u = [1, 0.8, 1.2]$, $\delta_z = [1, 0.5, 0.8]$ and ρ is equal for all SUs. We observe that as K increases, R_{LB}^* increases, since the possibility of energy overflow decreases and battery can store more energy.

Fig. 12 shows R_{LB}^* versus \bar{T}_{av} . For small \bar{T}_{av} , the AIC in (41) is active and the transmit power is limited by the interference constraint. As \bar{T}_{av} increases, SUs are allowed to transmit more power and the rate R_{LB}^* increases. However,

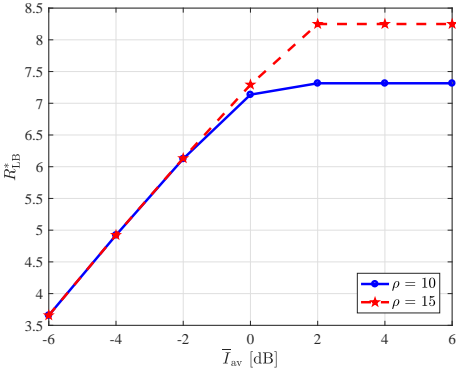


Fig. 12: R_{LB}^* versus \bar{I}_{av} for $N_u = 3, K = 80$.

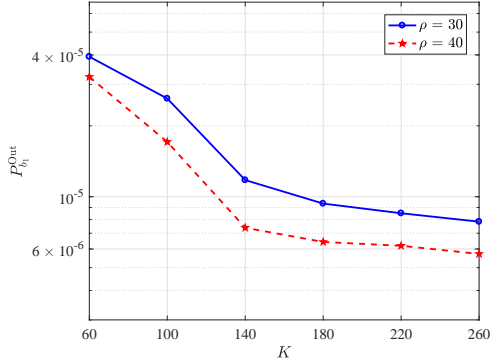


Fig. 13: $P_{b_1}^{\text{Out}}$ versus K for SU_1 when $\bar{I}_{av} = 2$ dB.

for large \bar{I}_{av} , the transmit power is restricted by the level of harvested energy, and increasing \bar{I}_{av} has no effect on the rate R_{LB}^* . Moreover, for small \bar{I}_{av} where AIC is active, increasing ρ has no effect on the R_{LB}^* . On the other hand, for large \bar{I}_{av} , if the harvest rate ρ increases, R_{LB}^* will increase. Fig 13 depicts $P_{b_1}^{\text{Out}}$ versus K for SU_1 where the parameters Ω_1 and θ_1 are obtained by maximizing R_{LB}^* and substituted in (43) to obtain $P_{b_1}^{\text{Out}}$. We observe that increasing the battery capacity leads to a lower battery outage probability

We define the transmission outage probability P_{α}^{Out} as the probability of SU_n not transmitting data to the AP due to the weak SU_n -AP channel or insufficient energy at the battery. We have

$$\begin{aligned} P_{\alpha_n}^{\text{Out}} &= \Pr(P_n = 0 | \hat{\mathcal{H}}_{0,n}) = \omega_{0,n} \Pr(P_n = 0 | \hat{\mathcal{H}}_{0,n}, \mathcal{H}_0) \\ &\quad + \omega_{1,n} \Pr(P_n = 0 | \hat{\mathcal{H}}_{0,n}, \mathcal{H}_1) \end{aligned} \quad (45)$$

where

$$\begin{aligned} &\Pr(P_n = 0 | \hat{\mathcal{H}}_{0,n}, \mathcal{H}_\varepsilon) \\ &= \sum_{k=0}^{\alpha_t} \zeta_{k,n} \Pr(\alpha_{k,n} = 0 | \hat{\mathcal{H}}_{0,n}, \mathcal{H}_\varepsilon, b_n \leq \alpha_t) \\ &\quad + \sum_{k=\alpha_t+1}^K \zeta_{k,n} \Pr(\alpha_{k,n} = 0 | \hat{\mathcal{H}}_{0,n}, \mathcal{H}_\varepsilon, b_n \geq \alpha_t+1) \end{aligned} \quad (46)$$

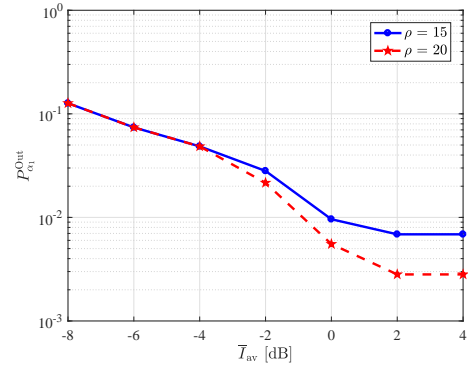


Fig. 14: P_{α}^{Out} versus \bar{I}_{av} for SU_1 when $K = 100$.

Substituting (3) and (46) in (45) we get

$$P_{\alpha_n}^{\text{Out}} = \sum_{k=0}^{\alpha_t} \zeta_{k,n} + \sum_{k=\alpha_t+1}^K \zeta_{k,n} Y_{k,n} \quad (47)$$

Fig. 14 shows $P_{\alpha_1}^{\text{Out}}$ versus \bar{I}_{av} for SU_1 where the parameters Ω_1 and θ_1 are obtained by maximizing R_{LB}^* and substituted in (47) to obtain $P_{\alpha_1}^{\text{Out}}$. We observe that with larger \bar{I}_{av} (before saturation), the SUs are allowed to use more power for data transmission and $P_{\alpha_1}^{\text{Out}}$ decreases. However, for large \bar{I}_{av} by increasing \bar{I}_{av} , $P_{\alpha_1}^{\text{Out}}$ remains constant since the transmit power is limited by the harvested energy.

VII. CONCLUSION

We consider an uplink CR network that can access a wideband spectrum licensed to a primary network, which is divided into non-overlapping narrowband channels. The SUs are equipped with a rechargeable battery of finite capacity and are aware of the available energy of their battery. There are error-free feedback channels from AP to SUs. SUs sense the activity of PU_{tx} and transmits data to AP if the channels are sensed idle. We formulated a constrained optimization problem, where the sum rate of SUs-AP link is maximized, subject to the average interference power constraint imposed on PU_{tx} and the battery causality constraint. We illustrated the effect of the AIC on the probabilities of the battery states and our CR system rate via simulation.

REFERENCES

- [1] T. Yucek and H. Arslan, "A survey of spectrum sensing algorithms for cognitive radio applications," *IEEE Communications Surveys Tutorials*, vol. 11, no. 1, pp. 116–130, First 2009.
- [2] A. Ali and W. Hamouda, "Advances on spectrum sensing for cognitive radio networks: Theory and applications," *IEEE Communications Surveys Tutorials*, vol. 19, no. 2, pp. 1277–1304, 2017.
- [3] H. Yazdani and A. Vosoughi, "On the spectrum sensing, beam selection and power allocation in cognitive radio networks using reconfigurable antennas," in *2019 53rd Annual Conference on Information Sciences and Systems (CISS)*, March 2019.
- [4] H. Yazdani, A. Vosoughi, and X. Gong, "Beam selection and discrete power allocation in opportunistic cognitive radio systems with limited feedback using ESPAR antennas," *IEEE Transactions on Cognitive Communications and Networking*, vol. 6, no. 1, pp. 325–339, 2020.
- [5] H. Yazdani, A. Vosoughi, and X. Gong, "Achievable rates of opportunistic cognitive radio systems using reconfigurable antennas with imperfect sensing and channel estimation," *arXiv:2007.04390*, 2020.

[6] S. Mao, M. H. Cheung, and V. W. S. Wong, "Joint energy allocation for sensing and transmission in rechargeable wireless sensor networks," *IEEE Transactions on Vehicular Technology*, vol. 63, no. 6, pp. 2862–2875, 2014.

[7] S. Yin, Z. Qu, and S. Li, "Achievable throughput optimization in energy harvesting cognitive radio systems," *IEEE Journal on Selected Areas in Communications*, vol. 33, no. 3, pp. 407–422, 2015.

[8] S. Biswas, S. Dey, and A. Shirazinia, "Sum throughput maximization in a cognitive multiple access channel with cooperative spectrum sensing and energy harvesting," *IEEE Transactions on Cognitive Communications and Networking*, vol. 5, no. 2, pp. 382–399, 2019.

[9] M. Ku, W. Li, Y. Chen, and K. J. Ray Liu, "Advances in energy harvesting communications: Past, present, and future challenges," *IEEE Communications Surveys Tutorials*, vol. 18, no. 2, pp. 1384–1412, 2016.

[10] H. Zhang, Y. Nie, J. Cheng, V. C. M. Leung, and A. Nallanathan, "Sensing time optimization and power control for energy efficient cognitive small cell with imperfect hybrid spectrum sensing," *IEEE Transactions on Wireless Communications*, vol. 16, no. 2, pp. 730–743, Feb 2017.

[11] L. Zhang, M. Xiao, G. Wu, S. Li, and Y. Liang, "Energy-efficient cognitive transmission with imperfect spectrum sensing," *IEEE Journal on Selected Areas in Communications*, vol. 34, no. 5, pp. 1320–1335, 2016.

[12] K. Wu, H. Jiang, and C. Tellambura, "Sensing, probing, and transmitting strategy for energy harvesting cognitive radio," in *2017 IEEE International Conference on Communications (ICC)*, May 2017, pp. 1–6.

[13] W. Chung, S. Park, S. Lim, and D. Hong, "Optimal transmit power control for energy-harvesting cognitive radio system," in *2013 IEEE 78th Vehicular Technology Conference (VTC Fall)*, Sep. 2013, pp. 1–5.

[14] A. Sultan, "Sensing and transmit energy optimization for an energy harvesting cognitive radio," *IEEE Wireless Communications Letters*, vol. 1, no. 5, pp. 500–503, October 2012.

[15] F. Zhang, T. Jing, Y. Huo, and K. Jiang, "Throughput maximization for energy harvesting cognitive radio networks with finite horizon," in *2017 9th International Conference on Wireless Communications and Signal Processing (WCSP)*, Oct 2017, pp. 1–7.

[16] G. Ardestiri, H. Yazdani, and A. Vosoughi, "Optimal local thresholds for distributed detection in energy harvesting wireless sensor networks," in *2018 IEEE Global Conference on Signal and Information Processing (GlobalSIP)*, Nov 2018, pp. 813–817.

[17] —, "Power adaptation for distributed detection in energy harvesting WSNs with finite-capacity battery," in *2019 IEEE Global Communications Conference (GLOBECOM)*, 2019, pp. 1–6.

[18] S. Park, H. Kim, and D. Hong, "Cognitive radio networks with energy harvesting," *IEEE Transactions on Wireless Communications*, vol. 12, no. 3, pp. 1386–1397, March 2013.

[19] S. Park and D. Hong, "Achievable throughput of energy harvesting cognitive radio networks," *IEEE Transactions on Wireless Communications*, vol. 13, no. 2, pp. 1010–1022, February 2014.

[20] D. Zhang, Z. Chen, J. Ren, N. Zhang, M. K. Awad, H. Zhou, and X. S. Shen, "Energy-harvesting-aided spectrum sensing and data transmission in heterogeneous cognitive radio sensor network," *IEEE Transactions on Vehicular Technology*, vol. 66, no. 1, pp. 831–843, 2017.

[21] H. S. Lee, M. E. Ahmed, and D. I. Kim, "Optimal spectrum sensing policy in RF-powered cognitive radio networks," *IEEE Transactions on Vehicular Technology*, vol. 67, no. 10, pp. 9557–9570, 2018.

[22] D. Niyato, P. Wang, and D. I. Kim, "Performance analysis of cognitive radio networks with opportunistic RF energy harvesting," in *2014 IEEE Global Communications Conference*, 2014, pp. 1096–1101.

[23] D. Altinel and G. K. Kurt, "Finite-state markov channel based modeling of RF energy harvesting systems," *IEEE Transactions on Vehicular Technology*, vol. 67, no. 2, pp. 1713–1725, 2018.

[24] X. Yang, M. Sheng, H. Sun, X. Wang, and J. Li, "Spatial throughput analysis and transmission strategy design in energy harvesting cognitive radio networks," *IEEE Transactions on Communications*, vol. 66, no. 12, pp. 5938–5951, 2018.

[25] S. Park, J. Heo, B. Kim, W. Chung, H. Wang, and D. Hong, "Optimal mode selection for cognitive radio sensor networks with RF energy harvesting," in *2012 IEEE 23rd International Symposium on Personal, Indoor and Mobile Radio Communications - (PIMRC)*, 2012, pp. 2155–2159.

[26] J. Yan and Y. Liu, "A dynamic SWIPT approach for cooperative cognitive radio networks," *IEEE Transactions on Vehicular Technology*, vol. 66, no. 12, pp. 11122–11136, 2017.

[27] F. Zhou, Z. Li, J. Cheng, Q. Li, and J. Si, "Robust AN-aided beam-forming and power splitting design for secure MISO cognitive radio with SWIPT," *IEEE Transactions on Wireless Communications*, vol. 16, no. 4, pp. 2450–2464, 2017.

[28] M. R. Zenaidi, Z. Rezki, and M. Alouini, "On communications under stochastic energy harvesting with noisy channel state information," in *2016 IEEE Global Communications Conference (GLOBECOM)*, 2016, pp. 1–6.

[29] R. Ma and W. Zhang, "Optimal power allocation for energy harvesting communications with limited channel feedback," in *2014 IEEE Global Conference on Signal and Information Processing (GlobalSIP)*, 2014, pp. 193–197.

[30] A. H. Sakr and E. Hossain, "Cognitive and energy harvesting-based D2D communication in cellular networks: Stochastic geometry modeling and analysis," *IEEE Transactions on Communications*, vol. 63, no. 5, pp. 1867–1880, 2015.

[31] M. Ku, Y. Chen, and K. J. R. Liu, "Data-driven stochastic models and policies for energy harvesting sensor communications," *IEEE Journal on Selected Areas in Communications*, vol. 33, no. 8, pp. 1505–1520, 2015.

[32] M. R. Zenaidi, Z. Rezki, and M. Alouini, "Performance limits of online energy harvesting communications with noisy channel state information at the transmitter," *IEEE Access*, vol. 5, pp. 1239–1249, 2017.

[33] J. F. Shortle, J. M. Thompson, D. Gross, and C. M. Harris, *Fundamentals of queueing theory*. John Wiley & Sons, 2018, vol. 399.

[34] R. Zhang, H. Chen, P. L. Yeoh, Y. Li, and B. Vucetic, "Full-duplex cooperative cognitive radio networks with wireless energy harvesting," in *2017 IEEE International Conference on Communications (ICC)*, 2017, pp. 1–6.

[35] X. Guo, Y. He, S. Atapattu, S. Dey, and J. S. Evans, "Power allocation for distributed detection systems in wireless sensor networks with limited fusion center feedback," *IEEE Transactions on Communications*, vol. 66, no. 10, pp. 4753–4766, 2018.

[36] H. Yazdani and A. Vosoughi, "On optimal sensing and capacity trade-off in cognitive radio systems with directional antennas," in *2018 IEEE Global Conference on Signal and Information Processing (GlobalSIP)*, Nov 2018, pp. 1015–1019.

[37] S. M. Kay, *Fundamentals of statistical signal processing*. Prentice Hall PTR, 1993.

[38] B. Hassibi and B. M. Hochwald, "How much training is needed in multiple-antenna wireless links?" *IEEE Transactions on Information Theory*, vol. 49, no. 4, pp. 951–963, April 2003.

[39] A. Vosoughi and A. Scaglione, "On the effect of receiver estimation error upon channel mutual information," *IEEE Transactions on Signal Processing*, vol. 54, no. 2, pp. 459–472, 2006.

[40] A. Vosoughi and Y. Jia, "How does channel estimation error affect average sum-rate in two-way amplify-and-forward relay networks?" *IEEE Transactions on Wireless Communications*, vol. 11, no. 5, pp. 1676–1687, 2012.